Atmos. Meas. Tech. Discuss., 7, 6625–6649, 2014
www.atmos-meas-tech-discuss.net/7/6625/2014/
doi:10.5194/amtd-7-6625-2014

Atmospheric Measurement Techniques Discussions

Humidity sensor failure: a problem that should not be neglected by the numerical weather prediction community

Y. Liu[1,2] **and N. Tang**[3]

[1]Numerical Weather Prediction Center, China Meteorological Administration, No.46 South Zhongguancun Street, Haidian District, Beijing 100081, China
[2]National Meteorological Center, China Meteorological Administration, No.46 South Zhongguancun Street, Haidian District, Beijing 100081, China
[3]College of Atmospheric Science, Nanjing University of Information Science and Technology, No.219 Ningliu Road, Nanjing 210044, China

Received: 23 March 2014 – Accepted: 4 June 2014 – Published: 4 July 2014

Correspondence to: Y. Liu (liuyan@cma.gov.cn)

Published by Copernicus Publications on behalf of the European Geosciences Union.

Abstract

In this paper, a new issue that very low relative humidity observations exist in a deeper atmosphere layer in the low- and mid-troposphere is studied on the basis of the global radiosonde observations from December 2008 to November 2009, and the humidity retrieval productions from Formosa Satellite mission-3/Constellation Observing System for Meteorology, Ionosphere, and Climate (FORMOSAT-3/COSMIC, referred to as COSMIC hereafter) in the same period. Results show that these extremely dry relative humidity observations are considerable universal in the worldwide operational radiosonde data. Globally, the annual average occurrence probability of the extremely dry relative humidity is of 4.2 %. These measurements usually occur between 20° and 40° latitudes in both Northern and Southern Hemispheres, and in the height from 700 to 450 hPa in the low- and mid-troposphere. Winter and spring are the favoured seasons for these extremely dry humidity observations, with the maximum ratio of 9.53 % in the Northern Hemisphere and 16.82 % in the Southern Hemisphere. The phenomenon is mainly related to the performance of the radiosonde humidity sensor and the cloud types traversed by the radiosonde balloon. These extremely low relative humidity observations are erroneous, which cannot represent the real atmospheric status, and are likely caused by the failure of humidity sensor. However, these observations have been archived as the formal data. It will affect the reliability of numerical weather prediction, the analysis of weather and climate, if the quality control procedure is not applied.

1 Introduction

Radiosonde is a highly important means of obtaining upper-air temperature, pressure, moisture and wind observation and has been used operationally for over 70 years. Although the accuracy of the radiosonde humidity sensor is gradually being improved, the quality of humidity observations has not been satisfied, particularly in the upper troposphere and lower stratosphere, wherein the sensor cannot detect high relative humidity

AMTD
7, 6625–6649, 2014

in cirrus clouds. A number of studies (e.g., analyses based on long-term observations) and the inter-comparisons of the radiosonde system by the World Meteorological Organisation (WMO) (i.e., tests involving hygrometers of the research radiosonde system and highly accurate chilled mirror humidity dew-point hygrometer flown together from one balloon) demonstrate the large errors of humidity observations (Li et al., 2012). These errors are related to the bad performance of the humidity sensor under low temperature and low humidity conditions, thus resulting in time-lag errors, sensor icing errors, sensor aging and contamination among others (Wang et al., 2003; Miloshevich et al., 2006; Vömel et al., 2007; Nash et al., 2010; Bian et al., 2011).

Although radiosonde hygrometers have been updated from gold beater skin hygrometers and carbon-film hygrometers to capacitive hygrometers, the previously mentioned problems have not been fully solved. Some studies have emphasised that operational radiosonde hygrometers using carbon hygristors fail to respond to humidity changes in the upper troposphere and middle troposphere; an example of such operational radiosonde hygrometers are US Sippican humidity sensors, which are unresponsive at heights where temperature is only −8 °C (Wang et al., 2003).

A new issue has recently emerged from Chinese L-band radiosonde relative humidity observation. The relative humidity profiles often indicate deep dry layers in the lower troposphere, and the observations show low relative humidity values (RHs < 2 %) at a given height and no response to humidity changes for a long time even to the end of the soundings (Fig. 1a). By contrast, some cases can recover with height (Fig. 1b). Zhang et al. (2010) suggested that such dramatic changes of the relative humidity do not comply with the atmospheric stratification law. Tang et al. (2014) showed that the dry layer observed in the Chinese L-band radiosonde system in the lower troposphere are unnatural anomalies. Although low RHs of less than 10 % are common in the troposphere (Spencer and Braswell, 1997; Zhang et al., 2003; Wang et al., 2010), the dry bias here will likely be a result of the erroneous data caused by humidity sensor failure, because the sensors entirely stop working at a certain altitude (a random altitude, but quite low). Tang et al. (2013) further showed that the dry bias phenomenon depends on

AMTD
7, 6625–6649, 2014

the performance of the humidity sensor and the cloud types encountered by the sensors. The humidity sensor will easily fail if the sounding instrument goes through deep and thick clouds, most of which are stratiformis clouds with high water vapour and an obvious dry layer, and is accompanied by atmospheric temperature stratification.

The occurrence percentage of dry bias in the Chinese L-band radiosonde system due to humidity sensor failure reaches 12.63 % in the survey (Tang et al., 2014). It is a serious problem that should not be neglected by the numerical weather prediction community. Does the relative humidity observation from other countries indicate the abnormal dry phenomenon caused by sensor failure? If so, how is the distribution and what are the causes? This study aims to answer these questions. The remainder of this paper is organised as follows. Chapter 2 describes the data and methods employed in this study. Chapter 3 details the survey on the failure of global operational radiosonde humidity sensors. Chapter 4 presents the comparison between radiosonde relative humidity observations and radio occultation (RO) observations. Chapter 5 shows the possible causes of the relative humidity observation failure. Chapter 6 is the conclusion and discussion.

2 Data and method

The radiosonde data used in this paper are dated between December 2008 and November 2009 and are obtained from the Global Telecommunication System. After excluding stations with less than 5 observations, a total of 844 radiosonde stations and 451 283 data are obtained. The method of Tang et al. (2013) is adopted to survey the failure of global operational radiosonde relative humidity observations. If the relative humidity profile with a value of less than 5 % continuously appears at the range of more than 200 hPa below the 300 hPa height, humidity sensor failure is assumed. We define the height under 300 hPa to highlight the new issue of humidity observation in the low and middle troposphere instead of the well-known old issue of dry bias in the high troposphere.

AMTD
7, 6625–6649, 2014

The RO data of the Constellation Observation System of Meteorology, Ionosphere and Climate (COSMIC) (Anthes et al., 2008) and the analysis results of the European Centre for Medium-Range Weather Forecasts (ECMWF) model at the same time period are used for inter-comparison. The matching method between RO and radiosonde data is similar to matching method implemented by Tang et al. (2013). The time window for the match is three hours before and after the radiosonde observation time, and the space window is in a 250 km × 250 km square grid at the centre of the radiosonde. If RO falls within the grid, radiosonde matching is confirmed. If multiple RO profiles are matched at the same time, we select the nearest RO profile.

Firstly, the Magnus saturation vapour pressure equation

$$e_s = \begin{cases} 6.112 \times \exp\left(\frac{17.62 \times t}{243.12 + t}\right) \times F(p) & \text{if } (t \geq -45) \\ 6.112 \times \exp\left(\frac{22.46 \times t}{272.62 + t}\right) \times F(p) & \text{if } (t < -45) \end{cases} \quad (1)$$

is used to calculate the saturation vapour pressure of the RO observation. Vapour pressure is then converted to relative humidity, where t represents the temperature in °C, and $F(p)$ is the enhancement factor related to atmospheric pressure:

$$F(p) = 1.0016 + 3.15 \times 10^{-6} \times p - \frac{0.074}{p}, \quad (2)$$

$$\mathrm{RH} = \frac{e}{e_s} \times 100\,\%. \quad (3)$$

To compare these data, we must convert the radiosonde data from a geopotential height to a geometric height coordinate by using the following equation:

$$z = \frac{a \times \bar{g} \times z_g}{g_0(\varphi, 0) \times a - \bar{g} \times z_g}, \quad (4)$$

where z represents the geometric height, z_g represents the geopotential height, a is the radius of the Earth at 6371 km, $\bar{g} = 9.80655\,\mathrm{m\,s^{-2}}$, which is the average at a 45°

AMTD
7, 6625–6649, 2014

latitude at sea level, $g_0(\varphi, 0)$ is the acceleration of gravity at latitude φ at sea level and

$$g_0(\varphi, 0) = 9.80620 \times (1 - 0.0026442 \cos 2\varphi + 0.0000058 \cos^2 2\varphi). \quad (5)$$

Finally, we use the cubic spline interpolation method to interpolate the radiosonde data to vertical layers with a resolution of 100 m, same resolution to the RO data.

3 Results

3.1 Global distribution of humidity sensor failures

Table 1 shows the number and ratio of all and failure relative humidity observations for four seasons. A total of 18 609 failure relative humidity observations among 447 021 observations are recorded between December 2008 and November 2009, and the percentage of failure observation is approximately 4.17 % worldwide. Table 1 shows that humidity sensor failure can occur at any time but mostly occurs during winter and spring for both hemispheres, with the highest percentage during winter at 9.53 % in the mid-latitude region of the Northern Hemisphere and 16.82 % in the mid-latitude region of the Southern Hemisphere. In the survey, 211 among 844 radiosonde stations have no failure observations; these stations are mainly located in the high-latitude regions of the Northern Hemisphere and in tropical regions.

Figure 2 shows the number of relative humidity sensor failure observations for each radiosonde station during the period of the survey. Different colour dots correspond to the number presented in the colour bar, and the black hollow circle indicates that no humidity sensor failure is observed. The failure observations mainly occur in the latitudes between 20° and 40° for both hemispheres. The number of failure observations is high in China, the United States, Australia, Western Europe and the east coast of South America. The problem in China is particularly serious with a maximus of 218 among 720 in Dalian station. However, the humidity sensor failure is rare in the tropical and high-latitude regions.

AMTD
7, 6625–6649, 2014

3.2 Characteristics of seasonal variation and vertical distribution

Figure 3 presents the statistics of relative humidity sensor failure observations for four seasons. As shown in the images, failure relative humidity observations occur mainly during spring and winter. Failure observations are less during the summer, and gradually increase during autumn. This trend is observed near 30° latitudes for both the Northern and Southern Hemispheres.

What is the vertical distribution characteristic of the failure relative humidity observations? Figure 4 shows the height and total station number, which satisfy the failure criterion. The height of most failure observations is between 700 hPa and 450 hPa and peaks at 700 hPa to 650 hPa followed by 500 hPa to 450 hPa. Failure observations may be seen under 900 hPa, which indicates humidity sensor failure may occur in the very low height.

4 Comparison with COSMIC/GPS RO data

Table 2 lists the number of all observations, failure observations and matched failure observations obtained by RO and three widely used operational instruments, Finland Vaisala, the US Sippican and the Chinese L-band radiosonde system, respectively. We calculate the bias and standard deviation for the failure, normal and all observations. Figure 5a shows the statistical results for all sondes in the entire year. Figure 5b–d presents the comparison of the results obtained by three instruments with COSMIC/GPS 1Dvar retrieval data. The number of failure observations is small on the global basis, thus resulting in the near superposition of the normal observation line (blue) and all observation line (red). Figure 5a also shows that the bias between normal and all observations is about ±5 % under 8 km height; thus, although COSMIC data has an error, the data are still in line with the WMO requirements on observation uncertainty and are suitable for cross-comparison. Compared with RO data, dry bias from failure data is larger than that in normal cases and the Maximus bias is beyond

AMTD
7, 6625–6649, 2014

−10 %. Figure 5b to d shows the similarity between Vaisala, Sippican and L-band humidity sensors to the COSMIC retrieval humidity data. However, the dry bias of Vaisala is smallest, whereas the dry bias of the Chinese L-band is large in the entire troposphere; this result is consistent with other research findings (Li et al., 2009; Sun et al., 2010; Bian et al., 2011).

Figure 6 illustrates two radiosonde relative humidity profiles in comparison with ECMWF analysis and RO data. The radiosonde observation, RO data and analysis generally have good consistency in the normal state. However, at the occurrence of a humidity sensor failure, the relative humidity drops from high moisture to low moisture quickly, and the sensor stops working entirely from a certain altitude. Although the RO and analysis profiles also experience a rapid decrease, the reduction will not be less than 10 % and the value will not remain constant, which indicates that temperature, pressure and humidity data based on 1Dvar are not subjected to the sensitivity of the sensors. Sometimes the humidity sensor can partly or fully recover as the balloon re-enters the clouds (Fig. 6b), including cirrus clouds, because the high moisture inside the clouds is helpful for sensor recovery. Figure 6 also illustrates that the abnormal dry phenomenon in the lower troposphere is unreasonable and that this phenomenon does not reflect the true state of the atmosphere.

5 Possible causes of humidity sensor failure

5.1 Performance of the sensor

Figure 7 shows the relative humidity and temperature profiles of six different failure sensors. As seen in the figures, the relative humidity observations decrease quickly in a short time from a high humidity value to below 5 % in the middle-lower troposphere and then maintains low humidity values. For example, the German Graw G sensor decreases rapidly from 93 % to 1 % from a height of 820 hPa to 787 hPa and then maintains low humidity values. Some sensors lose their sensing ability entirely (Fig. 7a

AMTD
7, 6625–6649, 2014

and d), whereas other sensors may recover. The relative humidity in all cases is over 87 %. When the value starts decreasing, an inversion temperature layer is observed, thus revealing the existence of clouds in these cases.

Figure 8 shows the distribution of the operational radiosonde stations worldwide. The different colours represent different humidity sensors. In contrast to Fig. 2, we find that all sensors are potential failures and most of them are carbon hygrometers. In the figure, the blue point represents the Vaisala sensor, which is widely used in Western Europe, Australia and South America. Although the Vaisala uses capacitive hygrometers and is recognised the best sensor, the number of failure observations is quite few. Therefore, instrument capability is not the only cause of sensor failure. However, the similarity between Figs. 8 and 2 indicates that instrument capability is always an important factor that should not be ignored. The capability of the Chinese L-band system is insufficient; hence, this sensor tends to exhibit significant problems.

5.2 Relationship to the atmospheric condition, especially clouds

Figure 9 presents the distribution of stratiform clouds and their temporal evolvement from the International Satellite Cloud Climatology Plan D2 data sets in the corresponding period. A low cloud belt exists near 30° in the Northern and Southern Hemispheres, which is consistent with Klein's results (1993). The failure relative humidity observations mainly occur at nearby 30° latitude in both hemispheres and are particularly obvious in winter. The results imply the connection between humidity sensor failure and stratiform clouds distribution.

Generally relative humidity is high inside stratiform clouds and low between two interbeds; and it decreases sharply at the top of clouds. The gradient of temperature stratification is close to that of the wet adiabatic process. The upper and top of the stratiform clouds usually have an inversion temperature layer that appears below the clouds at a height of 0.1 km to 0.2 km away from the top of the clouds (Shi, 2005). The examples provided in Sect. 5.1 indicate that the relative humidity of all radiosondes is over 87 % and decreases sharply with the existence of the inversion temperature layer

AMTD
7, 6625–6649, 2014

(Fig. 7). This phenomenon is supposed to occur similarly when the balloon emerges out of the stratiform clouds.

Wang et al. (2003) suggested that the sensor will lose sensitivity and stop responding in cold temperatures (approximately below −34 °C or above 8.5 km), or when relative humidity significantly changes within a short time. However, they did not analyse why relative humidity dramatically changes within a short time. From above analysis, we think that the dramatic changes of relative humidity occur after the balloon goes through the stratiform clouds, especially the wide range of stratiform clouds. The radiosonde balloon drifts during flying, and the horizontal scale of stratiform clouds is ten to thousands of kilometres, thus resulting that the horizontal distribution of the atmosphere is relatively uniform and stable, but the vertical distribution may exhibit dramatic changes. The horizontal scale of convective clouds is smaller, and the low humidity area is located inside cloud monomers. The balloon may repeatedly go through convective clouds from the sides instead of the tops. Therefore, the temperature and humidity profiles cannot depict the relatively uniform changes in the horizontal and drastic changes in the vertical for convective clouds.

6 Conclusion and discussion

According to the radiosonde data from December 2008 to November 2009, an issue that there exist quite more very low operational radiosonde relative humidity observations in the low- and middle-troposphere is studied, which has not been paid more attention. We calculated the percentage of their occurrence, compared these observations with other satellite products and reanalysis data, and analyzed the possible causes. The main conclusions are as follows:

(1) In the middle and lower troposphere, the deeply dry layer is often observed on the based of the relative humidity observations from the operational radiosonde system. This phenomenon is common. However, it is different from the dry layer in the natural variability, which exist in the troposphere, especially in the subtropics and extratropics

AMTD
7, 6625–6649, 2014

based on the previous studies (Spencer et al., 1997; Zhang et al., 2003; Wang et al., 2010); one of the most obvious features is that the relative humidity in our study has less change with time and has maintained in a very low value in a deep atmospheric layer, indicating that the hygrometer seems not respond the varation of the atmosphere. Globally, the annual average occurrence percentage of such dry humidity observations is approximately 4.2 %, and these observations mainly occur between the height of 700 and 450 hPa at 20° to 40° latitude for the Northern and Southern Hemispheres. The percentage is high, especially in winter, reaching 9.53 % in the middle altitudes of Northern Hemisphere and 16.82 % in the middle altitudes Southern Hemisphere, respectively.

(2) The reasons behind the extremely low relative humidity observations in the low- and middle-troposphere are the performance of the radiosonde humidity sensor and the cloud types in the atmosphere. When the balloon goes through the deep stratiform clouds with high moisture content, due to the huge changes in the external atmospheric conditions, the humidity sensor might be difficult to adapt, then fail and stop responding. The dramatical change of relative humidity in a short time further reveals the possible variation of the atmosphere state. But the internal physical mechanism of the humidity sensor failure is still needed investigation.

(3) The low relative humidity data that satisfy the criteria proposed by Tang et al. (2014) are erroneous. These data do not represent the real atmospheric status. However, they have been archived as formal records, and are widely used in atmospheric science research and services. If the data are used prior to correction and quality control, the reliability of the weather prediction and climate analysis will be significantly doubted. Therefore, there is an urgent need for taking effective measures to correct the erroneous data. It is noted that RO data and reanalysis can provide an effective tool to correct or to implement quality control for the failure observation.

Acknowledgements. This study was supported by the National Science Foundation of China (41075081) and the China Meteorological Administration Special Public Welfare Research Fund (GYHY201106008 and GYHY201206007).

AMTD
7, 6625–6649, 2014

References

Anthes, R. A., Bernhardt, P. A., Chen, Y., Cucurull, L., Dymond, K. F., Ector, D., Healy, S. B., Ho, S. P., Hunt, D. C., Kuo, Y.-H., Liu, H., Manning, K., McCormick, C., Meehan, T. K., Randel, W. J., Rocken, C., Schreiner, W. S., Sokolovskiy, S. V., Syndergaard, S., Thompson, D. C., Trenberth, K. E., Wee, T. K., Yen, N. L., and Zeng, Z.: The COSMIC/FORMOSAT-3 Mission-Early results, B. Am. Meteorol. Soc., 89, 313–333, 2008.

Bian, J., Chen, H., Vmel, H., Duan, Y., Xuan, Y., and Lv, D.: Intercomparison of humidity and temperature sensors: GTS1, Vaisala RS80, CFH, Adv. Atmos. Sci., 28, 139–146, 2011.

Klein, S. A. and Hartmann, D. L.: The seasonal cycle of low stratiform clouds, J. Climate, 6, 1587–1606, 1993.

Li, F., Li, B., and Wu, L.: An introduction of WMO 8th radiosondes inter-comparison and integrated remote instruments experiment, Advances in Earth Science, 27, 916–924, 2012 (in Chinese).

Li, W., Xing, Y., and Ma, S. Q.: The analysis and comparison between GTS1 radiosonde made in China and RS92 Radiosonde of Vaisala company, Meteological monthly, 35, 97–102, 2009 (in Chinese).

Miloshevich, L. H., Vömel, H., Whiteman, D., Lesht, B., Schmidlin, F. J., and Russo, F.: Absolute accuracy of water vapor measurements from six operational radiosonde types launched during AWEX-G and implications for AIRS validation, J. Geophys. Res., 111, D09S10, doi:10.1029/2005JD006083, 2006.

Moradi, I., Buehler, S. A., John, V. O., and Eliasson, S.: Comparing upper tropospheric humidity data from microwave satellite instruments and tropical radiosondes, J. Geophys. Res., 115, D24310, doi:10.1029/2010JD013962, 2010.

Nash, J., Oakley, T., Vömel, H., and Li, W.: WMO intercomparison of high quality radiosonde systems, World Meteorol. Org., Yangjiang, China, Tech. Rep., 2010.

Shi, A.: Progress in researches on microphysical characteristics and precipitation mechanisms of stratiform cloud precipitation, Meteorological Science and Technology, 2, 104–108, 2005 (in Chinese).

Spencer, R. W. and Braswell, W. D.: How dry is the tropical free troposphere? Implications for global warming theory, B. Am. Meteorol. Soc., 78, 1097–1106, doi:10.1175/1520-0477, 1997.

AMTD
7, 6625–6649, 2014

Sun, B., Reale, A., Seidel, D. J., and Hunt, D. C.: Comparing radiosonde and COSMIC atmospheric profile data to quantify differences among radiosonde types and the effects of imperfect collocation on comparison statistics, J. Geophys. Res., 115, D23104, doi:10.1029/2010JD014457, 2011.

Tang, N., Liu, Y., Li, G., and Li, F.: Preliminary analysis on abnormally dry phenomena of relative humidity observations of the Chinese L-band radiosonde system, J. Trop. Meteorol., in press, 2014 (in Chinese).

Vömel, H., Selkirk, H., Miloshevich, L., Valverde-Canossa, J., Valdés, J., Kyrö, E., Kivi, R., Stolz, W., Peng, G., Diaz, J. A.: Radiation dry bias of the Vaisala RS92 humidity sensor, J. Atmos. Ocean.-Tech., 24, 953–963, 2007.

Wang, J. H. and Rossow, W. B.: Determination of cloud vertical structure from upper air observations, J. Appl. Meteorol., 34, 2243–2256, 1995.

Wang, J. H., Cole, H. L., Carlson, D. J., Miller, E. R., Beierle, K., Paukkunen, A., and Laine, T. K.: Corrections of humidity measurement errors from the Vaisala RS80 radiosonde – application to TOGA COARE data, J. Atmos. Ocean. Tech., 19, 981–1002, 2002.

Wang, J. H., David, J. C., David, B. P., Terrence, F. H., Dean, L., Harold, L. C., Kathryn, B., and Edward, C.: Performance of operational radiosonde humidity sensors in direct comparison with a chilled mirror dew-point hygrometer and its climate implication, Geophys. Res. Lett., 30, 1860, doi:10.1029/2003GL016985, 2003.

Wang, J. H., Zhang, L. Y., Lin, P. N., Mark, B., Harold, C., Jack, F., Terry, H., Dean, L., Scot, L., Charlie, M., Joseph, V., Weng, C.-H., and Kathryn, Y.: Water vapor variability and comparisons in the subtropical Pacific from The Observing System Research and Predictability Experiment-Pacific Asian Regional Campaign (T-PARC) Driftsonde, Constellation Observing System for Meteorology, Ionosphere, and Climate (COSMIC), and reanalyses?, J. Geophys. Res., 115, D21108, doi:10.1029/2010jd014494, 2010.

WMO-NO: Guide to Meteorological Instruments and Methods of Observation, 2008 edition (7TH), Updated in 2010, Geneva, 2012.

Wolfgang, S., Claude, H., Schönenborn, F., Leiterer, U., Dier, H., and Lanzinger, E.: Pressure and temperature differences between Vaisala RS80 and RS92 radiosonde systems, J. Atmos. Ocean.-Tech., 25, 909–927, 2008.

AMTD
7, 6625–6649, 2014

Zhang, C. and Chen, J.: Contrast analysis of data observed by 59-type and L-band sonde, Journal of Shanxi Meteorology, 1, 29–31, 2010 (in Chinese).
Zhang, C. D., Mapes, B. E., and Soden, B. J.: Bimodality in tropical water vapour, Q. J. Roy. Meteorol. Soc., 129, 2847–2866, doi:10.1256/qj.02.166, 2003.

AMTD
7, 6625–6649, 2014

Table 1. Statistics of total and failure relative humidity observations.

Season	global		low-latitudes		mid-latitudes of NH		mid-latitudes of SH	
	Total	Failure (radio)	Total	Failure (radio)	Total	Failure (radio)	Total	Failure (radio)
DJF (Dec 2008–Feb 2009)	109 592	5996 (5.47 %)	13 748	734 (5.34 %)	48 345	4609 (9.53 %)	7327	363 (4.95 %)
MAM (Mar 2009–May 2009)	111 496	4402 (3.95 %)	14 040	332 (2.36 %)	48 905	3374 (6.90 %)	7492	503 (6.71 %)
JJA (Jun 2009–Aug 2009)	112 174	3837 (3.42 %)	15 242	572 (3.75 %)	48 863	1852 (3.79 %)	7242	1218 (16.82 %)
SON (Sep 2009–Nov 2009)	113 100	4374 (3.87 %)	15 824	499 (3.15 %)	49 442	3070 (6.21 %)	6654	563 (8.46 %)
One year (Dec 2008–Nov 2009)	446 362	18 609 (4.17 %)	58 854	2137 (3.63 %)	195 555	12 905 (6.60 %)	28 715	2647 (9.22 %)

AMTD
7, 6625–6649, 2014

Table 2. Statistics of all and failure relative humidity observations matched with COSMIC data for different sensors during December 2008 and November 2009.

Sensor	all observations total	all observations matched	failure observations total (ratio)	failure observations matched
All sensors	447 021	26 405	18 609 (4.17 %)	904
Vaisala	144 668	8586	5114 (3.53 %)	262
Sippican	59 607	3670	3347 (5.62 %)	191
L-band	61 736	2657	7796 (12.63 %)	321

AMTD
7, 6625–6649, 2014

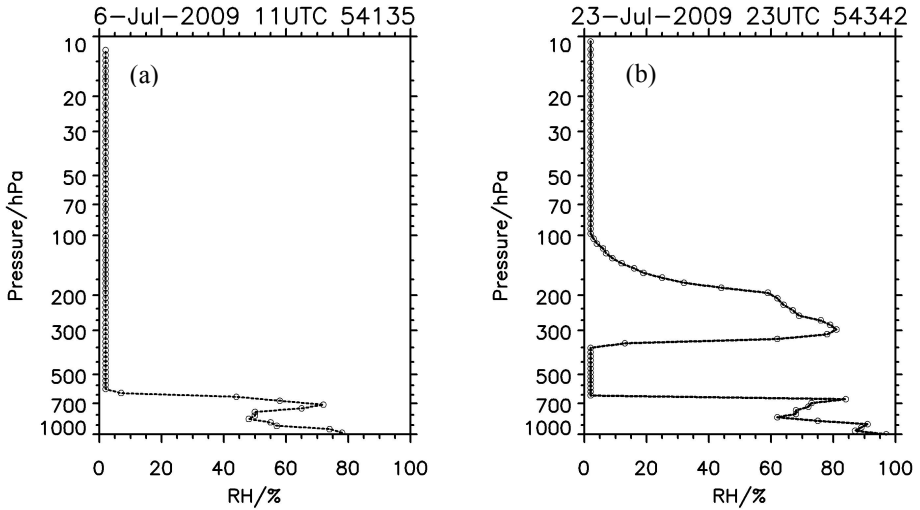

Figure 1. Two typical abnormally dry profile structures of relative humidity observation of the Chinese L-band radiosonde system, possibly caused by the humidity sensor failure (from Tang et al., 2014).

AMTD
7, 6625–6649, 2014

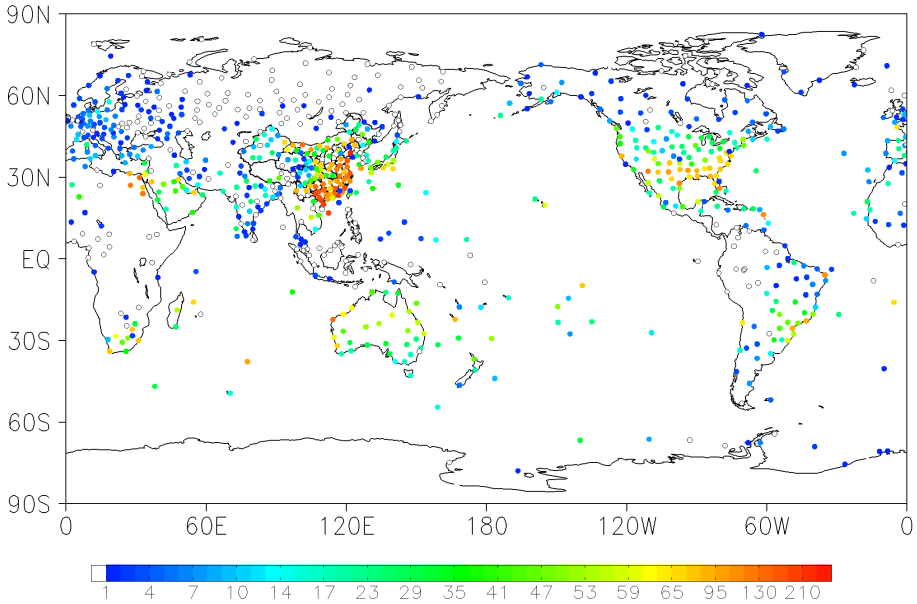

Figure 2. The global distribution character of total number of the failure relative humidity observations for each operational radiosonde station during December 2008 and November 2009. The colour dots correspond to the different number in the colour bar, and the black hollow circle denotes no humidity sensor failure observation.

AMTD
7, 6625–6649, 2014

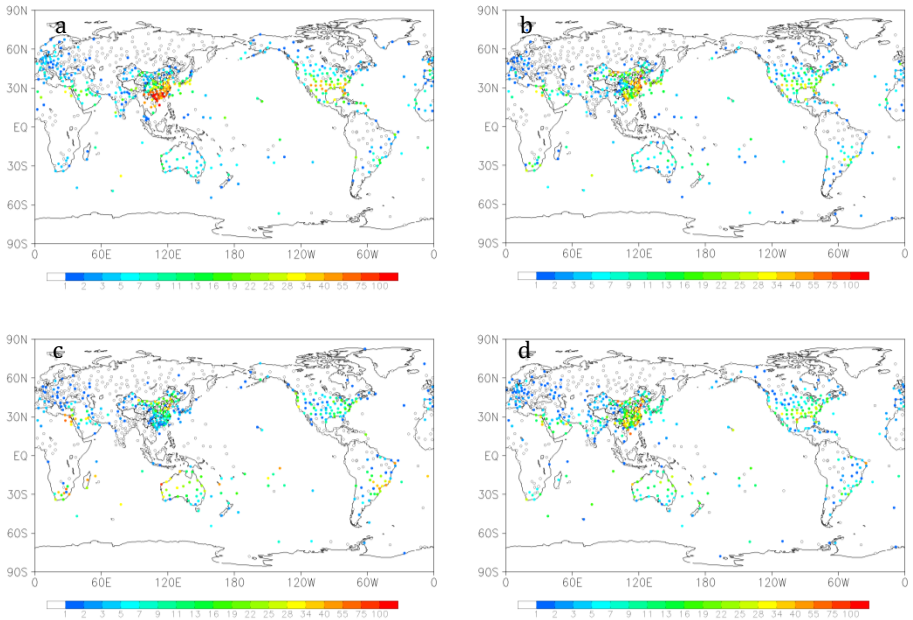

Figure 3. The Same as Fig. 2 but for four seasons. **(a–d)** represent for DJF (December, January and February), MAM (March, April and May), JJA (June, July and August) and SON (September, October and November), respectively.

AMTD
7, 6625–6649, 2014

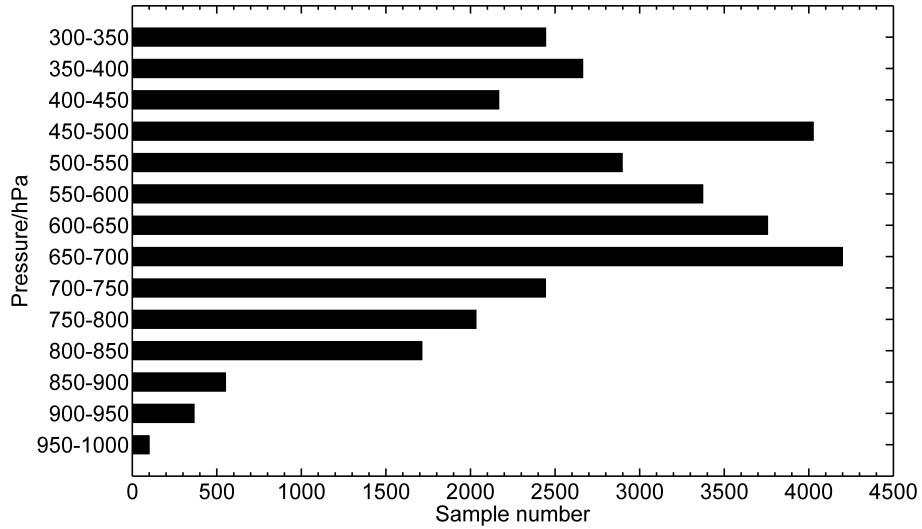

Figure 4. The vertical distribution of the failure relative humidity observations during December 2008 and November 2009. The *x* axis represents the number of relatively humidity observations, and the *y* axis presents the height with unit of hPa.

AMTD
7, 6625–6649, 2014

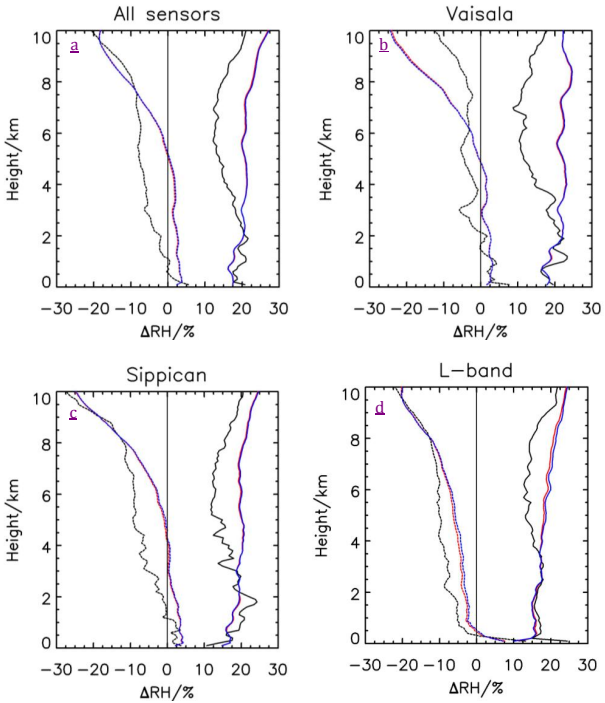

Figure 5. Bias (dashed) and standard deviation (solid) of the relative humidity data between the radiosonde observations and the COSMIC RO retrievals. The red lines represent all observations (not distinguish normal and abnormal observations), the blue lines represent the normal observations, and the black lines represent the false observations. (**a** and **b**) are the statistics for all data, Finland Vaisala, USA Sippican and China L-band radiosonde observation.

AMTD
7, 6625–6649, 2014

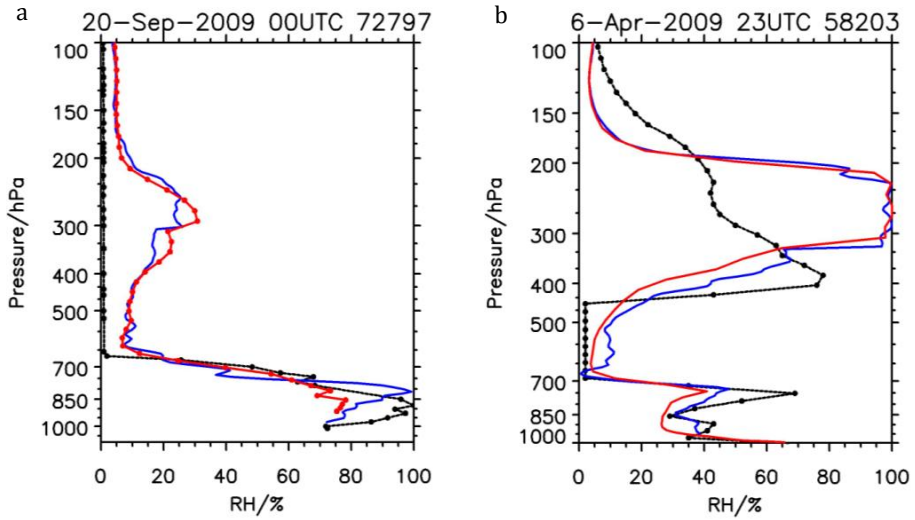

Figure 6. Comparison of the relative humidity profiles among the radiosonde (black), the COSMIC retrieval (blue) and ECMWF reanalysis (red). **(a)** represents the observation of station 72 797 at 00:00:00 UTC 20 September 2009; and **(b)** represents the observation of station 58 203 at 23:16:41 UTC 6 April 2009. The blue (red) lines represent the retrievals (reanalysis) matching the time and space criteria with the radiosonde observation.

AMTD
7, 6625–6649, 2014

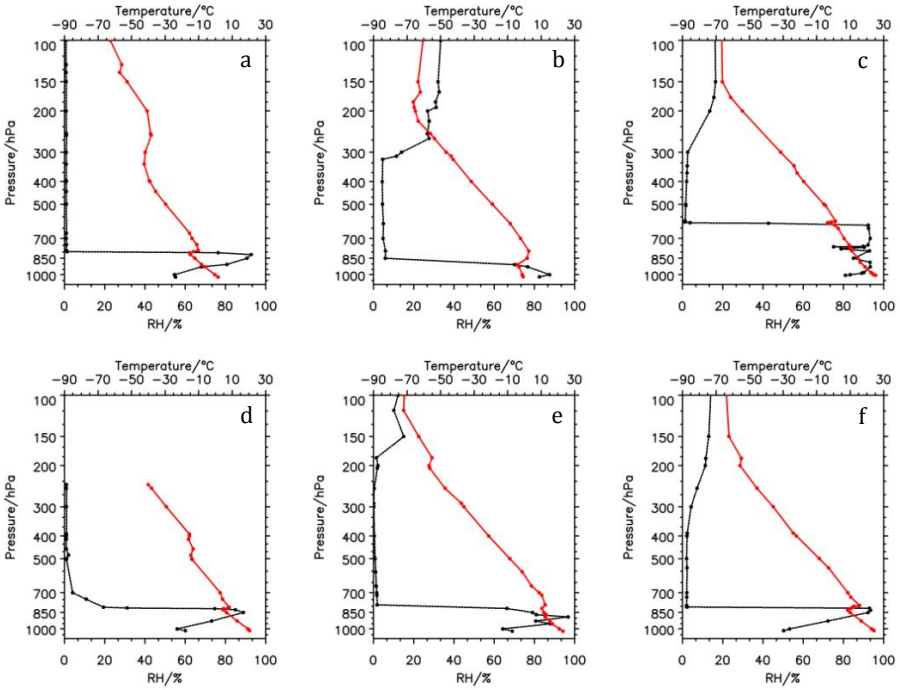

Figure 7. Relative humidity (black) and temperature (red) profiles for different types of radiosonde sensor. **(a–f)** are cases from Germany Graw Radiosonde G (station 47 185 at 12:00:00 UTC on 14 January 2009), Russia Meteorit MARZ2-type 2 (station 34 247 at 00:00:00 UTC on 26 October 2009), American VIZ-B2 (station 78 988 at 12:00:00 UTC on 17 December 2008), Japan's Meisei RS-016 (station 47 991 at 12:00:00 UTC on 7 February 2009), Finland Vaisala RS92 (station 83 746 at 12:00:00 UTC on 21 May 2009) and US Sippican MARK II (station 78 526 at 12:00:00 UTC on 10 March 2009).

AMTD
7, 6625–6649, 2014

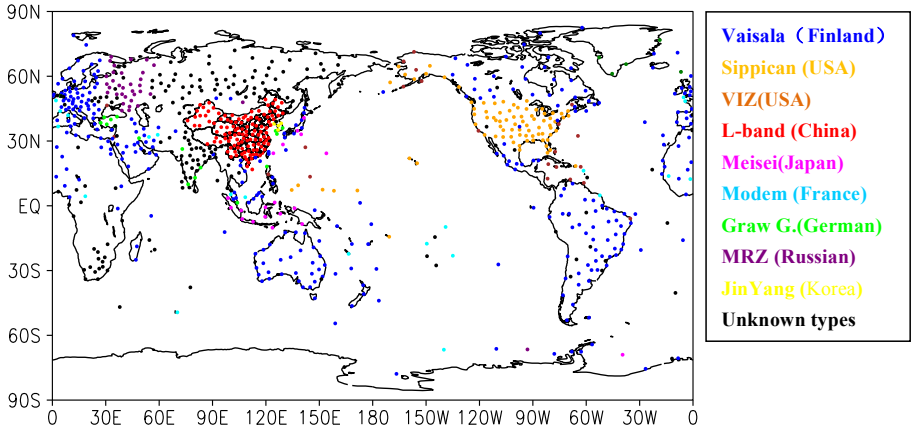

Figure 8. Distribution of radiosonde stations and the mainly operational radiosonde sensors.

AMTD
7, 6625–6649, 2014

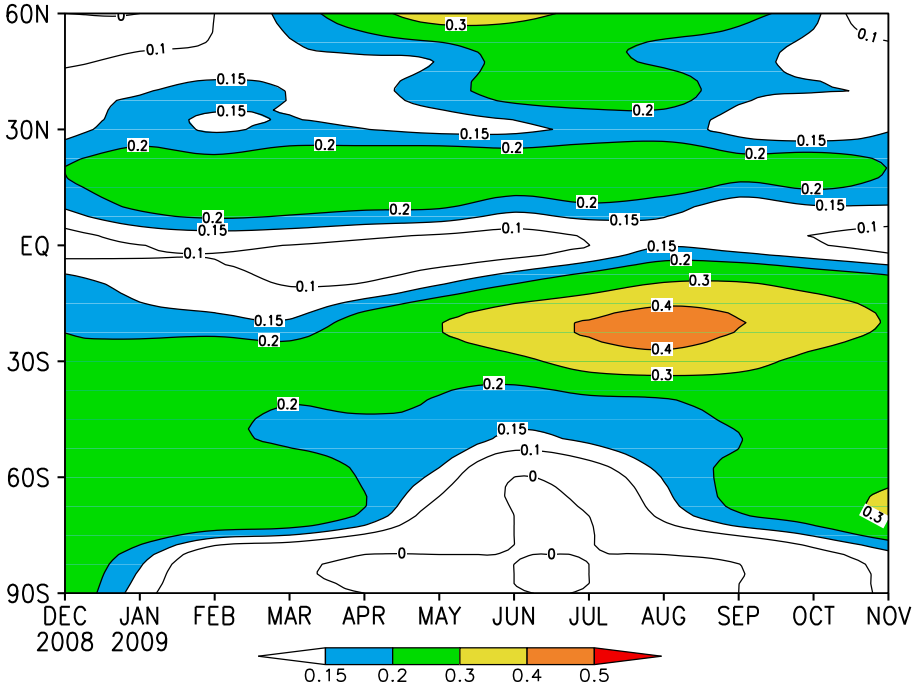

Figure 9. The average longitudinal distribution of stratiform clouds and its temporal evolvement during December 2008 and November 2009.

AMTD
7, 6625–6649, 2014